JACS
JOURNAL OF THE AMERICAN CHEMICAL SOCIETY
Article
pubs.acs.org/JACS

Monitoring Lipid Anchor Organization in Cell Membranes by PIE-FCCS

Sara B. Triffo,[†,‡,⊥,∥] Hector H. Huang,[†,‡,§,⊥] Adam W. Smith,[†,‡] Eldon T. Chou,[†] and Jay T. Groves*[,†,‡]

[†]Howard Hughes Medical Institute, Department of Chemistry, University of California, Berkeley, California 94720, United States
[‡]Physical Biosciences and Materials Sciences Divisions, Lawrence Berkeley National Laboratory, University of California, Berkeley, California 94720, United States
[§]Molecular & Cell Biology Department, University of California, Berkeley, California 94720, United States

Supporting Information

ABSTRACT: This study examines the dynamic co-localization of lipid-anchored fluorescent proteins in living cells using pulsed-interleaved excitation fluorescence cross-correlation spectroscopy (PIE-FCCS) and fluorescence lifetime analysis. Specifically, we look at the pairwise co-localization of anchors from lymphocyte cell kinase (LCK: myristoyl, palmitoyl, palmitoyl), RhoA (geranylgeranyl), and K-Ras (farnesyl) proteins in different cell types. In Jurkat cells, a density-dependent increase in cross-correlation among RhoA anchors is observed, while LCK anchors exhibit a more moderate increase and broader distribution. No correlation was detected among K-Ras anchors or between any of the different anchor types studied. Fluorescence lifetime data reveal no significant Förster resonance energy transfer in any of the data. In COS 7 cells, minimal correlation was detected among LCK or RhoA anchors. Taken together, these observations suggest that some lipid anchors take part in anchor-specific co-clustering with other existing clusters of native proteins and lipids in the membrane. Importantly, these observations do not support a simple interpretation of lipid anchor-mediated organization driven by partitioning based on binary lipid phase separation.

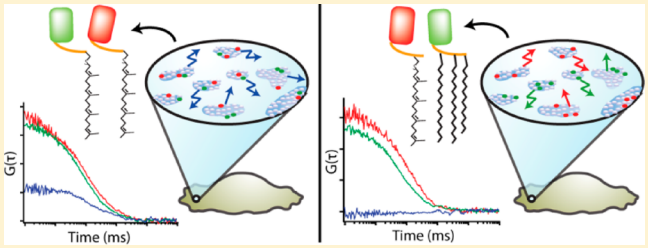

INTRODUCTION

Many proteins are anchored to cellular membranes through combinations of covalently attached lipid moieties.[1] These modifications, along with polybasic regions of the proteins, are known to be essential for proper subcellular localization, thereby regulating interactions between certain proteins.[2,3] It has been suggested that the anchors themselves contribute to the lateral organization of lipid-anchored proteins in the plasma membrane.[4−8] Proteins of the Ras family of small GTPases, for example, differ only in their anchors, but are sorted and targeted to different membrane microenvironments with different signaling effects.[9−12] In other instances, genetically or biochemically swapping one anchor type for another can disrupt protein function, even when proper subcellular localization is maintained.[13,14] These observations, among others, highlight the role that anchors play in the proper differential lateral sorting of lipid-anchored proteins in live cell membranes. There is as yet no consensus on the spatial targeting characteristics of the various anchor types in living cells, nor even if such a simple interpretation of anchor-mediated organization exists.[15−17]

Natural lipid anchors include isoprenyl groups, such as farnesyl and geranylgeranyl, and saturated fatty acids, such as palmitoyl and myristoyl.[18] Lipid-anchored proteins are often found to have multiple lipid modifications as well as basic amino acids near the anchor attachment point that aid in stabilizing the protein−membrane interaction, all of which we refer to here as the anchor. The different permutations of lipid modifications and basic amino acids give rise to a library of naturally occurring anchors with different chemical properties.

There is abundant evidence for the dynamic clustering and large scale spatial organization of membrane proteins, including lipid-anchored proteins in the cell membrane.[19−27] However, the role of the lipid anchor itself remains in question. Early studies of detergent-resistant membranes (DRMs) have suggested that palmitoylation can strongly bias the partitioning of proteins into tightly packed lipid domains.[7,28] However, the detergent solubilization disrupts the native organization and is a poor indicator of live cell membrane structures.[5,29−31] In giant unilamellar vesicles (GUVs) composed of synthetic or purified lipids and in giant plasma membrane vesicles (GPMVs), which are derived directly from cell membranes, lipid-mediated phase separation can be observed.[32−36] Compelling observations by fluorescence microscopy confirm that lipid anchors differentially sort into tightly packed liquid-ordered (Lo) domains enriched with saturated lipids and cholesterol, or liquid-disordered (Ld) domains, consisting of loosely packed unsaturated lipids.[37−39] However, the observed partitioning of lipid anchors between the phases is not consistent.[36] In the study by Johnson et al., the anchor of lymphocyte cell kinase (LCK) partitioned into the Lo domain in some GPMVs, into

Received: January 12, 2012
Published: May 25, 2012

   dx.doi.org/10.1021/ja300374c | J. Am. Chem. Soc. 2012, 134, 10833−10842

the Ld domain in others, and still in others resided equally in both domains.[40] Although GPMVs have a similar membrane composition as that of live cells, they lack cytoskeletal interactions and trafficking events which are likely to be important for regulating organization in live cell membranes.[36] Notably, the large-scale phase separation observed in GPMVs has not been observed in living cells.

Studies in live cell measurements should offer the most definitive answer to the question, yet evidence for anchor-specific membrane organization *in vivo* has also been inconclusive. Using Förster resonance energy transfer (FRET), Zacharias et al. studied the acylated anchors of both Lyn kinase and GAP-43 fused to FRET pairs of fluorescent proteins and concluded that these anchors cluster in a cholesterol-dependent manner in live MDCK cell membranes.[4] On the other hand, Glebov and Nichols studied similar chimeric constructs of GPI anchors and reported that they do not cluster and are distributed randomly in Jurkat and COS 7 cell membranes.[41] These studies arrive at different conclusions despite predictions that these anchors sort into the same small cholesterol-enriched domains in the membrane.[8,17,42,43] This discrepancy may be the result of the inherent limitations of FRET as a measure of membrane organization. Specifically, FRET requires a short separation between molecules and does not distinguish random collisions from clusters.

Other studies have examined the mobility of anchors in the membrane, such as Douglass et al. with single-particle tracking (SPT) and Kenworthy et al. with fluorescence recovery after photobleaching (FRAP).[44,45] While Douglass et al. reported that the LCK protein can sometimes be confined to nanoscopic domains, neither study reveals evidence that anchors were responsible for partitioning into stable domains.[44,45] Consequently, there is still confusion on the role of anchors in cell membrane organization.[15,17]

We employ pulsed interleaved excitation fluorescence cross-correlation spectroscopy (PIE-FCCS) to measure the degree to which chimeric anchors co-localize in live cell membranes.[4,6,46,47] In order to isolate the role of the anchor from protein−protein interactions, only the membrane anchor domain fused to either a red fluorescent protein, mCherry, or a green fluorescent protein, EGFP, is used (see Figure 1 and S6, SI Figure 1). FCCS measures the correlated movement of two fluorescent species as long as they are separated by a distance less than the detection area diameter (~0.4 μm).[48] PIE-FCCS provides cross-talk free cross-correlation, while fluorescence lifetime histograms from the same data stream allow simultaneous monitoring of FRET.[49] We examine the anchors in a pairwise manner, looking at co-localization of a single anchor type (labeled with two colors) or between two different anchor types. Our study considers whether interactions between these lipid anchors and membranes drive lateral organization and whether anchor identity defines differential sorting in the membrane.

In the following, we compare the organization of three chemically distinct lipid anchors taken from three different membrane proteins: (i) LCK, an immediate downstream activator of T cell receptor activation during the immune response, which has a N-terminal myristoylation and dual palmitoylations; (ii) the small GTPase, RhoA, with a C-terminal geranylgeranylation; and (iii) a member of the Ras oncogenic superfamily, K-Ras, with a similar C-terminal farnesylation. The saturated acyl chains of the LCK anchors contrast the bulky prenyl chains of the Ras and RhoA anchors, which differ from each other in length and sequence of the proximal basic amino acids.

The degree of two-color cross-correlation between lipid-anchored fluorescent proteins, measured with PIE-FCCS, investigates the degree of their co-diffusion in living cells. The results reveal varying degrees of cross-correlation between lipid anchors of the same type in membranes of Jurkat cells transfected with either RhoA anchors or LCK anchors at high-molecular densities (>2000 molecules/μm^2). In contrast, no co-localization of K-Ras anchors was detected at similar densities, despite having a C-terminal prenylation similar to the RhoA anchor. Significantly, co-localization between different anchors was never observed.

These findings suggest there are at least two distinct cluster types, into which the LCK and RhoA anchors selectively partition, existing in a background of various other membrane components. Furthermore, no significant decrease in the fluorescent lifetime of GFP is observed in any of these samples, regardless of the degree of co-localization. The clusters are not dense with fluorescent proteins, therefore they must also contain native membrane components.

Lipid-mediated binary phase separation inevitably leads to domains of the minority phase (e.g., rafts) in a background of the majority phase. Thus our observation of two orthogonally composed minority domains diffusing in a majority background is inconsistent with the concept that lipid anchors are partitioning into clusters based on lipid phase alone. We suggest that native cell membrane proteins play a dominant role defining the cluster content, possibly including or even nucleating lipid phase separation. Lipid-anchored fluorescent proteins partition into these pre-existing clusters based on mutual compatibility between the anchor and the overall cluster environment. Finally, we report that membrane organization is cell type specific; LCK and RhoA anchor pairs in COS 7 cell membranes exhibit minimal co-localization with themselves or with each other.

MATERIALS AND METHODS

Cloning: Construction of Truncated Lipid Anchor−Fluorescent Protein Fusion Genes. Constructs of EGFP-KRas-CT, mCherry-KRas-CT, mCherry-mGFP-KRas-CT in the pN1 vector with a strong CMV_{IE} promoter were given as gifts from Dr. Nick Endres and Dr. John Kuriyan (UC Berkeley). Retroviral plasmids containing LCK-NT-mCherry, LCK-NT-EGFP, mCherry-RhoA-CT, and EGFP-RhoA-CT were given as gifts from Dr. Björn Lillemeier and Dr. Mark Davis (Stanford). These genes were subcloned into the pN1 vector between the *Nco*I/*Not*I restriction sites. Polymerase chain reaction (PCR) primers and sequences of the genes can be found in the Supporting Information. All oligonucleotides were synthesized by Elim Bioscience (Fremont, CA) and sequenced by Elim Bioscience or the University of California Berkeley core DNA Sequencing Facility (Berkeley, CA)

Cloning: Construction of His-Tagged Fluorescent Proteins (FP-His12). Genes were cloned into the *Nco*I/*Xho*I restriction sites in the multiple cloning region downstream of a T7 promoter in the vector pET-28b(+) (Novagen). Genes for mCherry and mGFP were amplified by PCR and cloned into the *Nco*I/*Hin*dIII sites of pET-28b(+)-His12. mCherry-mGFP-His12 was constructed sequentially by first cloning mCherry into the *Nco*I/*Bam*HI sites of pET28b(+) with an oligo cassette encoding a 12× His-tag downstream of the fluorescent protein to generate pET-28b(+)-$mCherry_1$-His12. mGFP was then inserted into the *Bam*HI/*Hin*dIII sites of pET-28b(+)-$mCherry_1$-His12 to produce pET-28b(+)-$mCherry_1$-$mGFP_2$-His12. All cloning was carried out in *E. coli* XL1-Blue strain (Stratagene).

Protein Expression and Purification. FP-His12 proteins were expressed in *E. coli* BL21 Star (DE3) strain (Invitrogen). Expression

was induced during log phase growth with 1 mM isopropyl β-D-1-thiolgalatopyranoside (IPTG, Sigma) in 1 L suspension of Luria–Bertani bacterial media (Sigma) at 37 °C for 3–5 h. Cells were lysed by a freeze–thaw cycle, conventional treatment with 1 mg/mL lysozyme (Sigma) for 1 h at 4 °C in lysis buffer (40 mM Tris pH 7.4, 275 mM NaCl, 20 mM imidazole, 2% protease inhibitor cocktail for His-tag (Sigma)), and then by probe sonicator (Sonics & Materials Inc., VCX750). Samples were on ice during pulse sonication (5 s ON/9 s OFF, 150 s, amplitude = 35%, with a 3 mm stepped microtip). Lysate was clarified by addition of, and incubation with, nucleases (100 ng/mL RNaseA (Roche) and 25 ng/mL DNaseI (Roche)) and high-speed centrifugation (6000 rcf) for 45 min at 4 °C and then filtered through a 0.45 μm syringe filter. His-tagged proteins were purified by immobilized nickel affinity chromatography in a 1 mL His-Trap column on an AKTA Explorer (GE Life Sciences) and by gel filtration chromatography on a Superdex-100 HR size exclusion column (GE Life Sciences) in phosphate-buffered saline, pH 7.4 (PBS, Gibco, Cellgro), and 20% glycerol (EMD). Purified proteins were concentrated with Amicon centrifugal filters, flash frozen in liquid nitrogen in aliquots, and stored at −80 °C.

Supported Lipid Bilayer Formation and Protein Binding. Supported bilayers for empirical mapping of correlated states were made as previously described.[50,51] 1,2-Dioleoyl-*sn*-glycero-3-phosphocholine (18:1 (Δ9-Cis) DOPC) and 1,2-dioleoyl-*sn*-glycero-3-[(*N*-(5-amino-1-carboxypentyl)iminodiacetic acid)succinyl] (18:1 Ni-NTA DGS) were purchased from Avanti Polar Lipids and stored at −20 °C. Ni-NTA DGS (2 and 10 mol %, with 98 and 90 mol % DOPC, respectively) small unilamellar vesicles (SUVs) were prepared by sonication according to alternate protocol 1 in Lin et al.[50] Glass coverslip membrane supports (#1 Fisherbrand 25 mm round coverglass) are cleaned of organic contaminants by a 10 min submersion in highly oxidizing piranha etch solution (3:1 H_2SO_4:HOOH) thereby increasing the hydrophilicity of the support. Fifteen microliters of SUVs are mixed 1:1 with 2× Tris-buffered saline, pH 7.4 (TBS, Cellgro), and deposited on a clean, dry coverglass. Vesicles fuse to form a fluid supported bilayer on the coverglass. Coverslip and supported membranes are enclosed in a metal imaging chamber, and the bilayer must remain hydrated in order to maintain fluidity. The water is exchanged for 100 mM $NiCl_2$ in 2× TBS solution and incubated for 5 min in order to load the NTA with nickel ions. The solution is washed with filtered H_2O and then exchanged with 5 mL of 1× PBS. Next, 2, 6, and 10 mol % Ni-NTA DGS bilayers were incubated with ∼3, 6, or 9 nM mCherry-His12 and mGFP-His12 proteins in PBS for ∼30–40 min, after which all unbound proteins were washed away by exchanging the solution with 10 mL of PBS.

Cell Culture/Transfection/Sample Preparation. Jurkat T cells were cultured in RPMI1640 medium (Gibco) supplemented with 1 mM sodium pyruvate (Cellgro), 100 μg/mL penicillin/streptomycin (Cellgro), and 10% fetal bovine serum (FBS, Atlanta Biologicals). Cells were passaged every 2–3 days by seeding ∼10^6 cells in 5 mL of media in a T-25 cell culture flask and were disposed of after ∼15 passages. COS 7 cells were cultured in Dulbecco's Modification Eagle's Medium (4.5 g/L glucose DMEM, Cellgro) supplemented with 1 mM sodium pyruvate, 2 mM L-glutamine, and 10% FBS and passaged 1:20 at ∼95% confluency for up to 20 passages.

Cells were transiently transfected either 1 or 2 days before the experiment. COS 7 cells are seeded at a density of 250,000 cells/9.6 cm^2 well in a 6-well culture plate in 2.5 mL of reduced serum Opti-MEM I (Invitrogen) the day before transfection, while 10^6 Jurkat cells in 2.5 mL of Jurkat media are seeded in each well on the same day as transfection. For transfection, 2.5 μg of plasmid DNA was added to 250 μL of Opti-MEM I, and then 10 μL of lipofectamine 2000 transfection reagent (Invitrogen) was added to this mixture and incubated at room temperature for 30 min. This was then added to cells in six-well culture plates and incubated at 37 °C, 5% CO_2 for ∼12–36 h before the FCCS experiment.

To prepare Jurkat cells for data acquisition, cell culture media was exchanged twice with 5 mL of PBS, pH 7.4, prewarmed to 37 °C, by centrifuge (5 min, 250 rcf) and resuspended in 500 μL of HEPES buffered saline (pH 7.2) prewarmed to 37 °C and deposited on a poly-L-lysine-coated #1 coverglass (cleaned as before, and with 0.01% poly-L-lysine (P-L-L, Sigma) solution deposited on coverglass surface for 30 min, then aspirated) enclosed in a metal imaging chamber. Cells were allowed at least 15 min in the incubator in order to settle and adhere to the P-L-L coated coverslips. COS 7 cells were washed with 2 mL of prewarmed PBS, pH 7.4, and lifted from the surface by 1 mL of CellStripper (Cellgro) for 5–10 min, then resuspended with 500 μL of unsupplemented DMEM. Cells were centrifuged (5–10 min, 250 rcf), and the solution was aspirated. Remaining cells were resuspended in 500 μL of unsupplemented DMEM, added to P-L-L-coated coverslips in imaging chambers, and allowed at least 15 min in the incubator to adhere to the coverslips.

PIE-FCCS. FCCS measurements of lipid-anchored proteins in live cells were taken on a customized microscope setup. A Kr/Ar mixed gas laser (Stabilite 2018-RM, Newport Corp., Irvine, CA) provides a wavelength of 568 nm, while a pulsed diode laser (LDH-P-C-485, PicoQuant, Berlin, Germany) provides a 479 nm wavelength. For FCCS, the 568 and 479 nm lines are combined and coupled into a single-mode optical fiber. As the combined beams exit the fiber, they are collimated with an achromatic objective lens (Leica, 10×) and directed via a custom polychroic mirror (Chroma Technology Corp., Rockingham, VT) into the optical path of the microscope (TE2000E, Nikon Corp., Tokyo, Japan). A 100× TIRF oil objective, NA 1.49 (Nikon Corp., Tokyo, Japan), focuses down the excitation beam. The fluorescence is collected through the same objective and passed through a custom notch filter (Semrock, Rochester, NY) to remove any scattered laser light. The emitted light is then passed through a 50 μm confocal pinhole (Thorlabs, Newton, NJ). A 580 nm long-pass beamsplitter then splits and directs the emitted light toward two avalanche photodiodes (APDs) (SPCM-AQRH-16, Perkin-Elmer, Canada). Short-pass (550 nm) and band-pass (645/75 nm) optical filters (Chroma Technology Corp., Rockingham, VT) for the green and red channels, respectively, further select for proper wavelengths. A time-correlated single photon-counting (TCSPC) card (PicoQuant, TimeHarp 200, Berlin, Germany) collects signal from the APDs through a universal router (PRT 400, TTL SPAD router, PicoQuant, Berlin, Germany). The power of each laser was measured before entering the optical path of the microscope and was kept between 0.9 and 1.5 μW. Measurements were taken with the lasers pulsing at 10 MHz. The cw Kr/Ar beam is also pulsed at 10 MHz using an electro-optic modulator (EOM, 350-160 KD*P series, ConOptics) to give 18 ns pulses. The pulsing of the EOM and the diode laser is controlled and synchronized by a pulse generator (Quantum Composers, 9530 series). A delay of about 50 ns is set between the diode pulse and the EOM to ensure that the fluorescence completely decays between excitation pulses.

Cells with similar intensities in GFP and mCherry epi-fluorescent channels were selected for FCCS. When taking FCCS measurements, areas of the cell with obvious background fluorescence from proteins inserted into membranes of organelles or intracellular vesicles were avoided. The bottom membrane of the cell was brought into focus, which was maintained with an active focus stabilizer (Perfect Focus System, Nikon Corp., Tokyo, Japan). We measured up to five 15 s measurements in three to five spots in each cell for all samples. The cell samples were kept at room temperature for data acquisition and were observed for no more than 1.5 h.

Lifetime Acquisition. Fluorescence data for lifetime analysis were gleaned from the FCCS data set or acquired from separate samples (e.g., for cells expressing LCK-NT-EGFP only). Lifetime histograms were constructed from 15–120 s traces and were tail-fit with SymphoTime software (SymphoTime 5.1.3, PicoQuant, Berlin, Germany).

RESULTS AND DISCUSSION

FCCS Measures Co-diffusion of Anchor Constructs in Live Cell Membranes. Jurkat and COS 7 cells were transiently transfected with pairs of green and red lipid-anchored fluorescent protein constructs, and each transfection sample produced a broad distribution of expression levels. As

shown in Figure 1 (and S6, SI Figure 1), epi-fluorescent images of transfected cells reveal a spatially homogeneous distribution

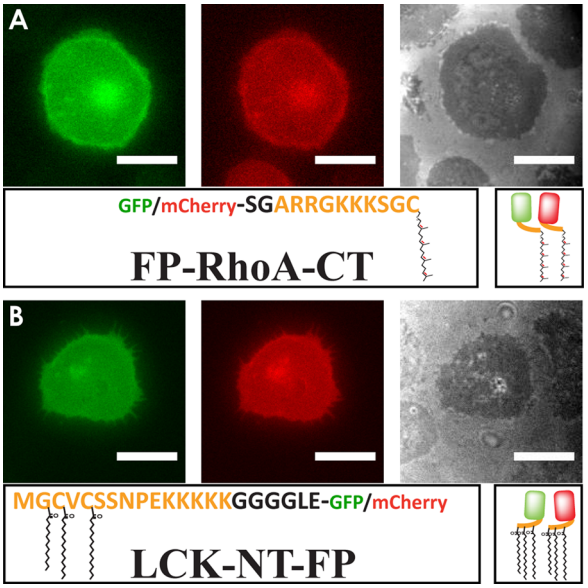

Figure 1. Green, red epi-fluorescent, and reflection interference contrast microscopy (RICM) images of Jurkat cells expressing (A) EGFP-RhoA-CT and mCherry-RhoA-CT and (B) LCK-NT-EGFP and LCK-NT-mCherry. Anchored fluorescent proteins are localized to the plasma membrane, and bright masses are due to intracellular organelles. RICM shows that cell membranes are well adhered to P-L-L-coated coverslips. Images are false-colored, and the scale bar is 10 μm. Cartoons detailing the lipid moiety and peptide sequence fused to EGFP or mCherry are shown below the images.

of fluorescent proteins in the plasma membrane. The lipid-anchored fluorescent fusion proteins described here are similar in design to those used in other studies.[4,40,44,45,52]

PIE-FCCS is used to detect dynamic co-localization of GFP and mCherry lipid-anchored constructs in live cells. This technique requires no fixation of cells or extraction of cell membranes, and measurements do not perturb the native organization of the membrane. Additionally, FCCS probes co-localization at length scales from several nanometers up to the diameter of the excitation spot (~0.4 μm), which goes below the resolution of conventional fluorescence microscopy (~200 nm) and beyond the practical range of FRET (up to ~10 nm). An observation of cross-correlation indicates dynamic co-localization and requires no *a priori* knowledge of the spatial length of organization.[53,54]

Auto-correlation of the fluorescence fluctuations (Figure 2C,E) resulting from movement of fluorophores through the excitation area is calculated by the normalized auto-correlation function in eq 1,

$$G(\tau) = \frac{\langle \delta I(t)\delta I(t+\tau)\rangle}{\langle I\rangle^2} + 1 \quad (1)$$

where $\delta I(t)$ is the fluctuation in fluorescence intensity at time t, and τ is the lag time. Two-color fluorescence cross-correlation is expressed similarly in eq 2, and gives the correlation between fluctuations from two different fluorescent signals,

$$G_x(\tau) = \frac{\langle \delta I_r(t)\delta I_g(t+\tau)\rangle}{\langle I_r\rangle\langle I_g\rangle} + 1 \quad (2)$$

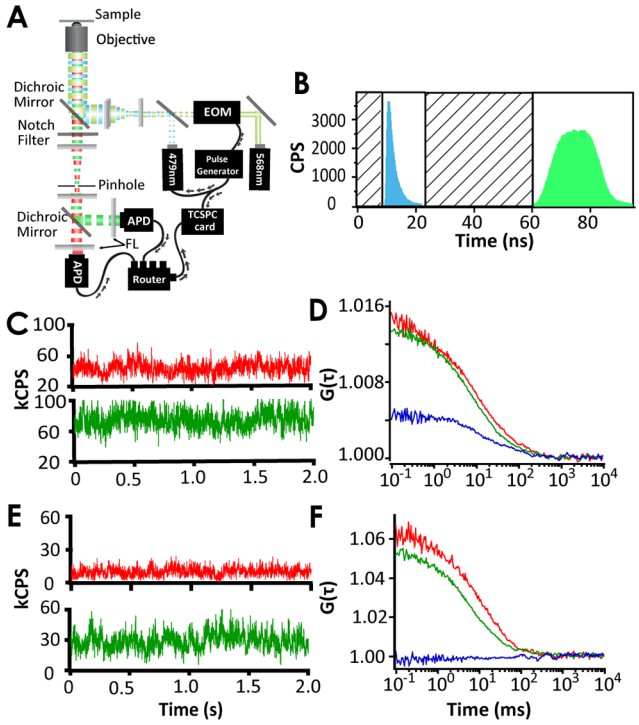

Figure 2. (A) Schematic of our PIE-FCCS microscope setup. (B) Arrival time (time-resolved) histogram of APD A (green) and APD B (cyan). Photons with arrival times within the diagonal lined boxes are removed before auto- and cross-correlation curves are calculated. (C) Intensity traces from APD A (red) and APD B (green) resulting from detected fluorescence from a bilayer sample with mCherry-mGFP-His12 exhibiting correlated diffusion. (D) Auto- (red and green) and cross-correlation curves (blue) calculated from the intensity traces in (C). (E) Intensity traces from a bilayer sample with mCherry-His12 and mGFP-His12 exhibiting uncorrelated diffusion. (F) Auto- and cross-correlation curves calculated from traces in (E).

where $\delta I_r(t)$ and $\delta I_g(t)$ are the fluctuations in fluorescence intensity of mCherry in channel A and GFP in channel B, respectively.

While the $G(\tau)$ intercepts of the auto-correlation curves of red and green species, $G_r(0)$ and $G_g(0)$, are inversely proportional to the concentration of diffusing red and green species in the excitation spot, respectively, the intercept of the cross-correlation curve, $G_x(0)$, is directly proportional to the concentration of species with both red and green fluorophores.[48,54] Here, the measure of cross-correlation is expressed as F_{cross}, which is defined in eq 3.[54]

$$F_{cross} = \frac{G_x(0) - 1}{(\min\{G_r(0), G_g(0)\}) - 1} \quad (3)$$

Pulsed-interleaved excitation and time-gating of data, as shown in Figure 2 B, eliminates artificial cross-correlation due to spectral bleed-through from the broad emission spectrum of GFP.[47] The auto- and cross-correlation curves were calculated from the reconstructed, time-gated intensity traces using a multiple-tau algorithm implemented in Matlab (The MathWorks, Inc.).[55] Data from a single spot were averaged before fitting. Intensity traces with large and irregular fluctuations or resulting in correlation curves showing long and irregular decays were discarded, as these irregularities are usually the result of membrane fluctuations or diffusion of intracellular vesicles into the excitation area. FCS and FCCS data were fit by

dx.doi.org/10.1021/ja300374c | J. Am. Chem. Soc. 2012, 134, 10833−10842

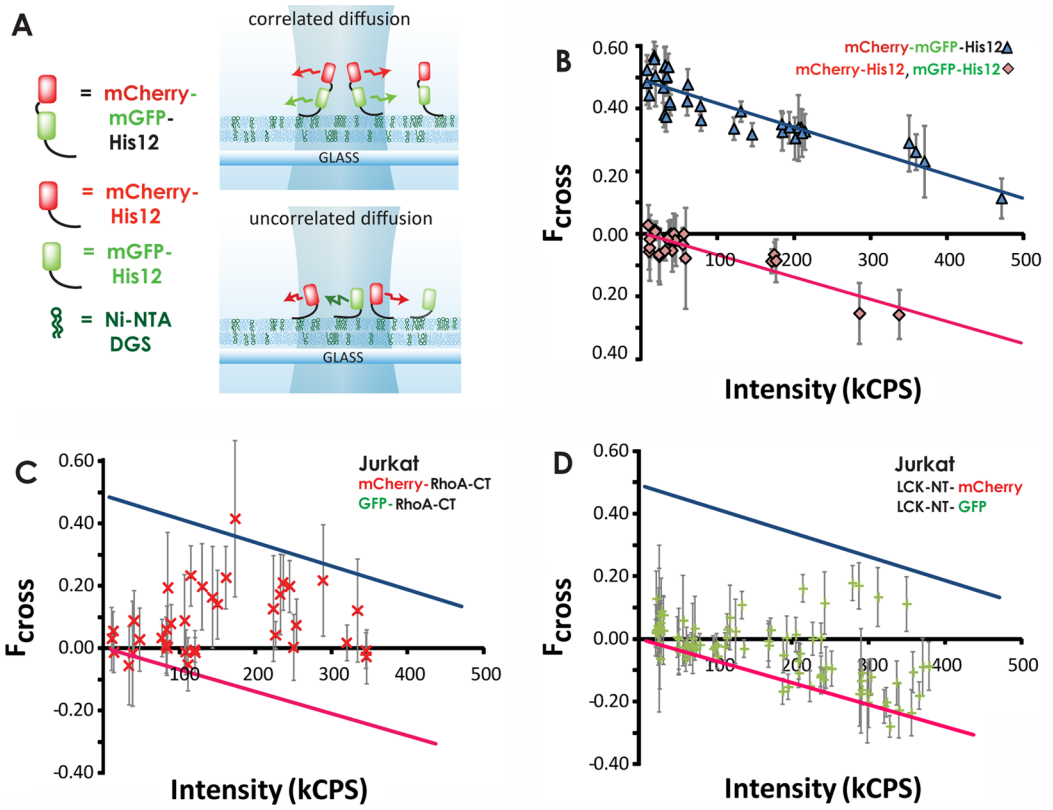

Figure 3. (A) Schematic of mCherry-mGFP-His12 diffusing on a Ni-NTA-DGS-containing supported lipid bilayer representing the correlated state (top) and mCherry-His12 and mGFP-His12 diffusing independently on a supported lipid bilayer representing the uncorrelated state (bottom). (B) Scatter plot of F_{cross} versus intensity of correlated mCherry-mGFP-His12 (blue ▲) and uncorrelated mCherry-His12 and mGFP-His12 (pink ◆). Increased intensity comes from increased surface density of His-tagged fluorescent proteins. Decreasing cross-correlation with respect to intensity is due to TCSPC card dead time and is fit to a linear trend. (C,D) EGFP-RhoA-CT/mCherry-RhoA-CT cross-correlation (red ×) and LCK-NT-EGFP/LCK-NT-mCherry cross-correlation (green +) with respect to increasing intensity in Jurkat cells. Blue and magenta lines represent the linear fits of the empirically mapped cross-correlation states from (B). Error bars represent the standard deviation of $G(0)$ at each spot.

finding the average of the earliest ten points for an accurate $G(0)$ value.[46]

Relative Correlation Is Scaled to Known Standards. To better represent the amount of cross-correlation present in the transfected cells, F_{cross} is empirically mapped, *in vitro*, with physical standards of polyhistidine-tagged fluorescent proteins on supported lipid bilayers corresponding to known states of correlated movements. Representative auto- and cross-correlation curves of these correlated and uncorrelated states are shown in Figure 2D and F, respectively, and these standards are illustrated in Figure 3A. F_{cross} of mCherry-mGFP-His12 samples, where the movement of each red fluorescent protein is entirely correlated with that of a green fluorescent protein, is the maximum F_{cross}, whereas F_{cross} of the uncorrelated mCherry-His12 and mGFP-His12 samples is the minimum.

Increased intensity from increased density of fluorophores results in linearly decreasing and even negative F_{cross} values, as seen in Figure 3B. The decrease in F_{cross} with respect to the total intensity from both detection channels can be attributed to the dead time of the TCSPC acquisition card.[47] Photons arriving during a dead time, when the TCSPC card is busy processing a signal, are not recorded, and this results in anti-correlation between GFP and mCherry at short lag times.[47] The TCSPC card has a longer dead time (~350 ns) than more conventional correlation cards or detection electronics.[56] SI Figure 3 shows an example of the anti-correlation in samples in uncorrelated states. This effect has been corrected by empirically mapping our correlated and uncorrelated boundaries (Figure 3B) using standards with total intensities ranging between 0 and 500 kCPS (kilocounts per second). The measured F_{cross} values of fluorescently labeled anchor pairs in all cell samples fall between the minimum (magenta line) and maximum (blue line) empirical boundaries of cross-correlation, as shown in Figure 3C,D. FCCS data from live cells are normalized to relative correlation values between 0 and 1 with respect to the minimum and maximum F_{cross} boundaries, as shown in Figure 4.

The molecular brightness of GFP and mCherry can also be determined from these *in vitro* control FCCS measurements. According to the two-dimensional diffusion model in eq 4,

$$G(\tau) = \frac{1}{N}\left(1 + \frac{\tau}{\tau_D}\right)^{-1} + 1 \tag{4}$$

the intercept of the function at $\tau = 0$, $G(0)$ of the auto-correlation function, is inversely proportional to the number, N, of diffusing species in the excitation spot. Since these polyhistidine-tagged fluorescent proteins have been engineered to be monomeric, the N measured by FCS in the uncorrelated control sample refers to the average number of fluorescent proteins detected.[4,57] The molecular brightness is calculated by dividing the average intensity for each channel by the number of fluorescent proteins of each color.

dx.doi.org/10.1021/ja300374c | J. Am. Chem. Soc. 2012, 134, 10833−10842

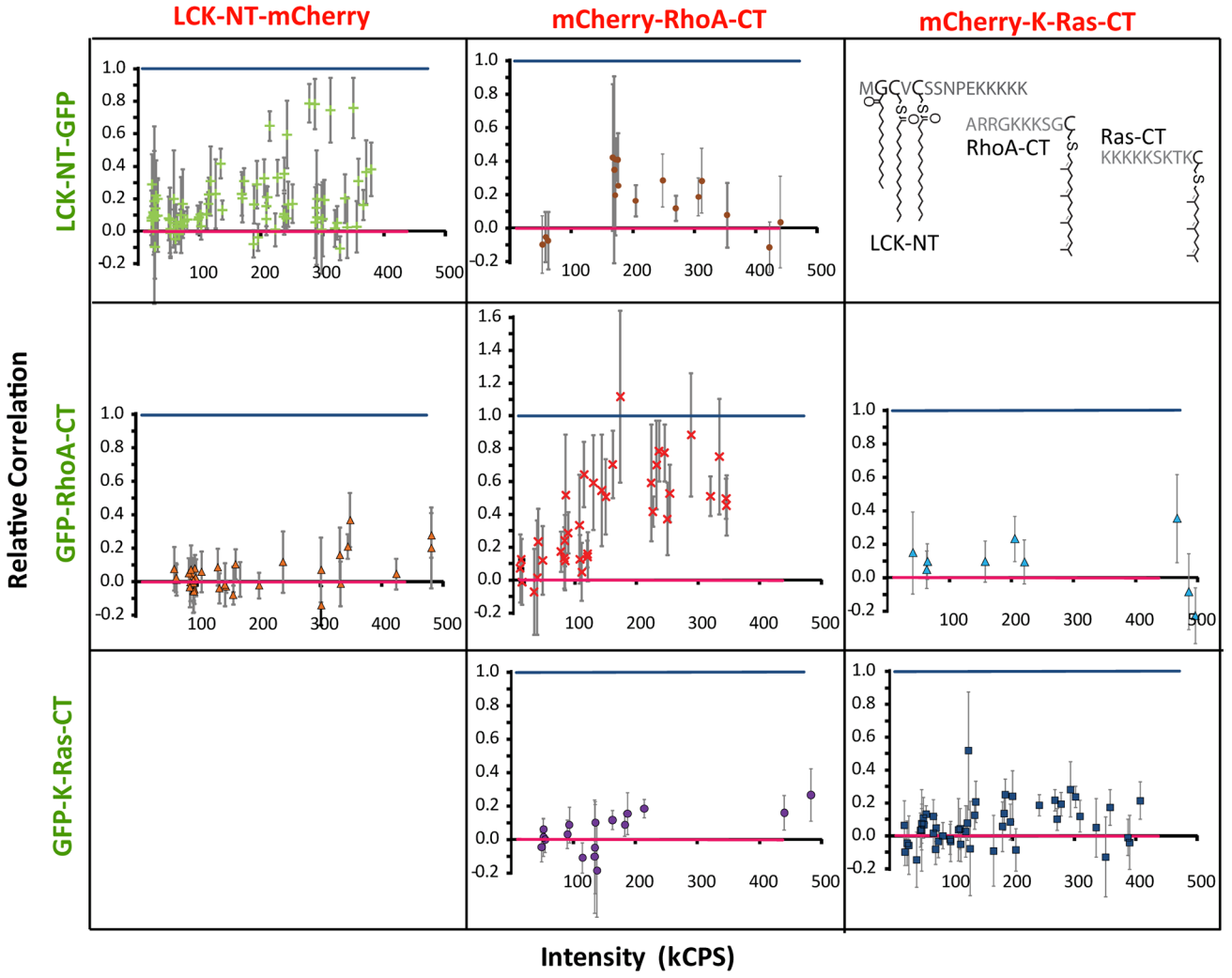

Figure 4. Normalizing cross-correlation to the empirically mapped correlated (1, blue) and uncorrelated (0, magenta) states for (top row, left to right) LCK-NT-EGFP/LCK-NT-mCherry (N = 87, 28 cells) (green +) and LCK-NT-EGFP/mCherry-RhoA-CT (N = 17, 5 cells) (brown ●), (middle row, left to right) EGFP-RhoA-CT/LCK-NT-mCherry (N = 36, 11 cells) (orange ▲), EGFP-RhoA-CT/mCherry-RhoA-CT (N = 37, 11 cells) (red ×), and EGFP-RhoA-CT/mCherry-K-Ras-CT (N = 9, 3 cells) (blue ▲), and (bottom row, left to right) EGFP-K-Ras-CT/mCherry-RhoA-CT (N = 17, 5 cells) (purple ●) and EGFP-K-Ras-CT/mCherry-K-Ras-CT (N = 49, 13 cells) (blue ■) in Jurkat T cells. Error bars represent the normalized standard deviation of $G(0)$ for each spot.

In live cell experiments the N obtained from FCCS measurements does not necessarily reflect the actual number of fluorescent proteins due to the many possible clustering states of lipid-anchored fluorescent proteins. Instead the actual density of lipid-anchored fluorescent proteins (ρ) is determined by dividing the overall fluorescence intensity by the molecular brightness of each fluorophore, determined as described above, and the area of the excitation spot (~0.1 μm^2), which is measured by fitting the auto-correlation curve for standard fluorophores of known diffusion constants.

Relative Correlation of Anchors in Cells Is Dependent on Density. In Jurkat cells expressing RhoA-CT-anchored fluorescent proteins, relative cross-correlation varies from cell to cell but increases with increasing fluorescence intensity in the membrane (Figure 4, row 2 column 2, data from four experiments, 11 cells), where intensity is proportional to concentration of fluorescent proteins in the cell membrane. At low fluorescent RhoA-CT intensities, the relative correlation matches that of the uncorrelated state, but it rises to the maximum correlation boundary at high intensities. The presence of relative cross-correlation indicates that RhoA-CT anchors co-diffuse and exist in clusters.

Examination of a different anchor pair, LCK-NT-mCherry and LCK-NT-EGFP, reveals a similar trend (Figure 4, row 1 column 1, data from seven experiments, 28 cells). However, the relative cross-correlation does not increase as much as the RhoA-CT anchors, and the distribution of cross-correlation values is more heterogeneous at high densities of LCK-NT anchors.

Relative Correlation Is Anchor Specific. PIE-FCCS measurements between different anchor types, LCK-NT-mCherry/EGFP-RhoA-CT and mCherry-RhoA-CT/LCK-NT-EGFP (Figure 4, row 2 column 1, and row 1 column 2, data from five experiments, 16 cells), show no cross-correlation regardless of the intensity of either fluorophore or which anchor is attached to GFP or mCherry. This indicates that RhoA-CT and LCK-NT do not partition into the same clusters.

Additionally, PIE-FCCS measurements of Jurkat cells expressing mCherry-K-Ras-CT/EGFP-K-Ras-CT (see S6, SI Figure 1) do not reveal cross-correlation within our range of

dx.doi.org/10.1021/ja300374c | J. Am. Chem. Soc. 2012, 134, 10833−10842

observation (Figure 4, row 3 column 3, data from four experiments, 13 cells). Similarly, the pairwise measurements of K-Ras-CT anchor and RhoA-CT anchor, which both possess isoprenyl modifications, do not exhibit any cross-correlation (Figure 4 row 3 column 2, and row 2 column3, data from three experiments, 8 cells).

In the case of LCK-NT and RhoA-CT anchors, the positive relative correlation among anchors of the same type is evidence that anchor interactions with the membrane can determine the lateral targeting of anchored proteins in the cell membrane. On the other hand, the absence of cross-correlation between any two different anchor types (including K-Ras-CT) reveals that all three anchor types prefer microenvironments that do not overlap with one another.

Relative Correlation Is Cell Specific. In fibroblast-like COS 7 cells, PIE-FCCS measurements of the RhoA anchors (S7 SI Figure 2C, data from three experiments, 6 cells, $N = 21$), and the LCK anchors (S7 SI Figure 2D, data from three experiments, 10 cells, $N = 38$) do not exhibit the same level of cross-correlation as seen in Jurkat cells; RhoA-CT anchors do not exhibit any cross-correlation while LCK-NT anchors show a very slight degree of cross-correlation. The absence of measured cross-correlation within the same range of intensities as that measured in Jurkat cells suggests that RhoA-CT anchors do not diffuse in clusters in COS 7 membranes. The difference in membrane organization is likely due to the differing membrane compositions and cell functions between the two cell types.[58,59]

Fluorescence Lifetimes Show No Energy Transfer. Analysis of the fluorescence lifetime of the GFP-anchored proteins in our cross-correlation experiments is shown in Figure 5. The time-tagged time-resolved (TTTR) data acquisition format allows the same photon data set acquired from PIE-FCCS to be used to generate fluorescence lifetime histograms in order to examine nanometer scale clustering via FRET.[54]

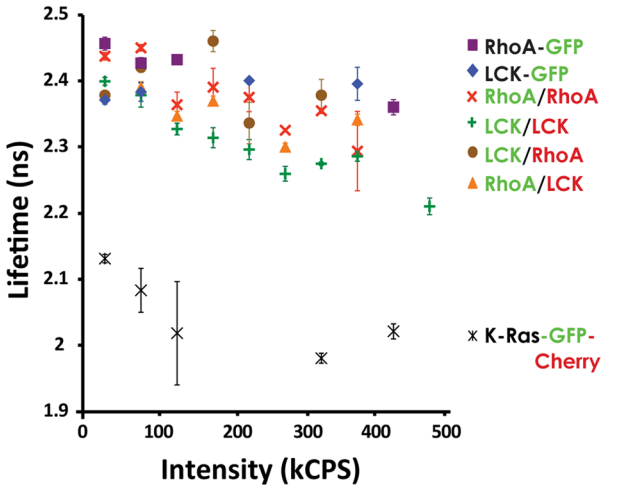

Figure 5. Fluorescence lifetimes were fit, and the fitted lifetimes were binned into 50 kCPS bins. The error bars represent the standard error of all points in each bin. Cells transfected with anchored GFP and anchored mCherry show the same decreasing trend with increasing intensity as cells transfected with only anchored GFP (LCK-NT-EGFP and EGFP-RhoA-CT). The difference in lifetime of the GFP when fused to mCherry in the single polypeptide mGFP-mCherry-K-Ras-CT, which we expect to undergo FRET, and that of the GFP in all other samples, shows that none of the other anchored GFPs undergo significant energy transfer.

Shortened GFP lifetimes are an indication of FRET between GFP and mCherry, indicating close proximity of two anchors. Cells transfected only with GFP-anchored proteins and, therefore, absent of a FRET acceptor serve as negative controls, while cells transfected with mCherry-mGFP-K-Ras-CT, where the covalent connection between GFP and mCherry guarantees close proximity, are positive controls for the presence of FRET. All cells transfected with a pair of GFP and mCherry anchors show GFP lifetimes similar to cells expressing only LCK-NT-EGFP or EGFP-RhoA-CT indicating no energy transfer due to FRET between mCherry and GFP. The exception is the positive control, mCherry-mGFP-KRas-CT, which has a distinctly shortened lifetime as evidence of FRET. Due to the dead time effect of the TCSPC card, there is a slight decreasing trend in lifetimes of all samples as the detected intensity increases. Decreasing the excitation power mitigates the dead time effect in SI Figure 5, revealing that LCK-NT-EGFP lifetime in LCK-NT-EGFP/LCK-NT-mCherry and LCK-NT-EGFP only transfected cells are still similar and remains consistent across a range of anchor densities.

These results show that FRET experiments alone would not have unambiguously detected RhoA-CT or LCK-NT anchor co-localization in this density range and emphasize the importance of using PIE-FCCS to investigate the organization of these anchors in the membrane.[17,45]

Anchors Partition into Specific Clusters. The cross-correlation results show that RhoA-CT and LCK-NT anchors exist in clusters exclusive of each other, while the absence of FRET between anchored fluorescent proteins in clusters suggests that the clusters are not densely packed with anchors. The likeliest explanation is that these anchors partition into pre-existing compatible clusters of native proteins and lipids in the membrane. The data show that an anchor density threshold must be overcome before any cross-correlation between anchored fluorescent proteins is detected. The density threshold is determined by the number of clusters into which the anchors have to sort. With fewer domains, the chance of having two different colored anchors in the same domain is greater at the same density than with a larger number of domains.

To quantify the difference in the trends of cross-correlation with increasing density between RhoA-CT and LCK-NT, in Figure 6, we use the calculated density of anchored probes to compare the distribution of relative correlation to a model that assumes that correlation is strictly the result of a probabilistic distribution of anchored probes into existing clusters in the cell membrane, as described by eq 5:

$$P_{\text{total}} = \sum_{N=0}^{\infty} \frac{N}{\langle N \rangle} \frac{\langle N \rangle^N \, e^{-\langle N \rangle}}{N!} \left(1 - \left(\frac{1}{2}\right)^{(N-1)}\right) \qquad (5)$$

where $\langle N \rangle$ is the average number of probes in a cluster (see S11 for a detailed description of the model). Using a least-squares fit of the model to our data, we determine the average number of clusters, n, where $n = \rho/\langle N \rangle$, or the density divided by the average number of probes in the cluster. In the case of the RhoA anchor data, we find there is a minimum of 1640 clusters/μm^2 ($R^2 = 0.593$). This value represents a lower bound to the number of clusters because the intensity of brighter samples is likely under-detected due to the dead time of the TCSPC card. We are also limited from measuring cross-correlation at higher membrane densities because FCCS is less sensitive at higher concentrations.[54]

dx.doi.org/10.1021/ja300374c | J. Am. Chem. Soc. 2012, 134, 10833−10842

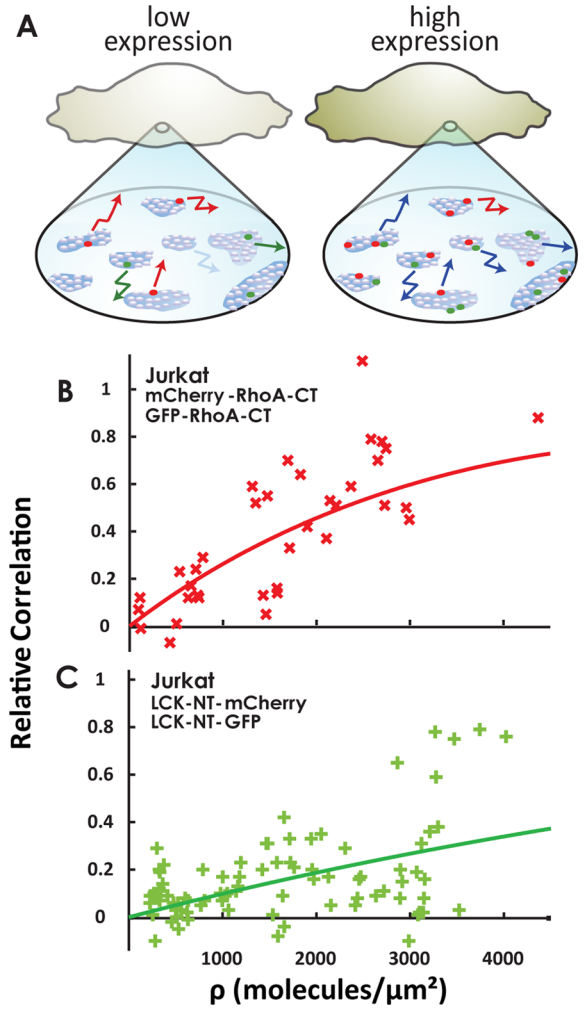

Figure 6. (A) Our model of RhoA-anchored fluorescent proteins sorting into pre-existing clusters based on a minimum density requirement before observing cross-correlation. (B,C) Relative cross-correlation of (B) mCherry-RhoA-CT/EGFP-RhoA-CT and (C) LCK-NT-mCherry/LCK-NT-EGFP with respect to the total surface density of anchored fluoroscent proteins in Jurkat cell membranes. A probablistic model (shown as a solid line) is fit to the distribution of relative correlation values to return the average number of clusters for each anchor type in the cell membranes, 1640 clusters/μm^2 (R^2 = 0.593) and 4820 clusters/μm^2 (R^2 = 0.2358) for (B) and (C), respectively.

The best fit of the probabilistic model to the LCK-NT cross-correlation measurements returns a cluster density of ~4800 clusters/μm^2 (R^2 = 0.2358), on average. Quantifying the cluster density allows us to quantitatively compare the relative correlation between RhoA-CT and LCK-NT anchors and according to our model, we find that there are more LCK-NT anchor-specific clusters than RhoA-CT anchor-specific clusters in Jurkat cell membranes.

Anchor Organization Is More Complex Than Phase Separation. Based on these observations, we present a more complex picture of the cell membrane than has been predicted by earlier models of membrane organization. The conventional model posits the existence of nanometer-scale phase-separated lipid domains in living cells known as lipid rafts.[8,52,60,61] Raft domains are believed to be enriched in cholesterol and sphingolipids, and their formation is often thought to be driven by Lo and Ld phase separation, although these requirements have been debated. According to this conventional raft model, lipid anchors with saturated acyl chains, such as the LCK anchor, are expected to cluster into Lo raft domains, while isoprenylated anchors, like the RhoA anchor, would be excluded from these domains without clustering.[14] While data from studies employing recent technological advances in superresolution techniques like photo-activated localization microscopy (PALM) and stimulated emission depletion (STED) FCS have hinted at greater heterogeneity in the species of clusters in the membrane, the discussion is, for the most part, still confined to describing organization within the context of a simple binary raft model that is based on disruptive detergent extraction methods and employs inappropriate terms such as "raft" marker and "non-raft" marker.[62,63]

While lipids and proteins are capable of large-scale phase separation in GPMV experiments, this mode of molecular sorting is insufficient to describe the level of organizational complexity seen in our live cell experiments. Rather, lipid-anchored fluorescent proteins partition into pre-existing clusters that are primarily defined by specific protein−protein and protein−lipid interactions among native cell membrane proteins. While this does not exclude the possibility that the clusters include or nucleate lipid phase separation, phase separation alone cannot generate the two orthogonally composed clusters into which RhoA-CT and LCK-NT partition among a background containing K-Ras-CT and many other membrane components. In this way, the membrane generates distinct environments capable of discriminating between the anchors.

■ CONCLUSIONS

PIE-FCCS has allowed a unique view of a complex and highly specific organizational scheme of the live cell membrane without relying on *a priori* knowledge of the composition of membrane clusters. FCCS reveals coordination of lipid anchors that would not have been determined from fluorescence lifetime analysis.

Here we show the existence of at least two distinct, non-overlapping domains that LCK-NT anchors, RhoA-CT anchors, and K-Ras-CT anchors recognize in a background of many other protein clusters in the membrane of Jurkat cells. The interactions between anchors and the cellular plasma membrane, which includes interactions between the charged residues of the anchor and negatively charged lipid head groups, lead to differential sorting of the anchors in a complex and heterogeneous organizational scheme that is incompatible with binary phase separation of the lipid raft model.[42,64] Moreover, the differential sorting between the RhoA and K-Ras anchors, despite their chemical similarities, is evidence that the sorting mechanism discriminates beyond just the saturation level of the lipid moiety of the anchor. The difference in FCCS results between COS 7 and Jurkat cell membranes indicates that membrane organization is cell specific. Taken together, this is evidence for a more complex level of organization in cell membranes than is normally considered.

■ ASSOCIATED CONTENT

Ⓢ Supporting Information

Gene sequences, supporting figures, and an explanation of the probability distribution model used. This material is available free of charge via the Internet at http://pubs.acs.org.

AUTHOR INFORMATION

Corresponding Author

jtgroves@lbl.gov

Present Address

[‖]McMichael Science Building 327B, 2625 Campus Box, Elon University, Elon, NC 27244

Author Contributions

[⊥]S.B.T. and H.H.H. contributed equally to this work,

Notes

The authors declare no competing financial interest.

ACKNOWLEDGMENTS

The authors acknowledge Il-Hyung Lee and Michael Coyle for contributions of Matlab analysis scripts. The authors also thank Ann Fischer from the MCB Tissue Culture Facility at UC Berkeley for obtained mammalian cell cultures, Dr. Nick Endres and Dr. John Kuriyan for K-Ras anchor-containing plasmids, and Dr. Björn Lillemeier and Dr. Mark Davis for access to LCK and RhoA anchor-containing plasmids. Finally, the authors thank Howard Hughes Medical Institute. This work was supported by the Director, Office of Science, Office of Basic Energy Sciences, Chemical Sciences, Geosciences and Biosciences Division of the U.S. Department of Energy under Contract No. DE-AC02_05CH11231.

REFERENCES

(1) Bhatnagar, R. S.; Gordon, J. I. *Trends Cell Biol.* **1997**, *7*, 14.
(2) Engelman, D. M. *Nature* **2005**, *438*, 578.
(3) Resh, M. D. *Nat. Chem. Biol.* **2006**, *2*, 584.
(4) Zacharias, D. A.; Violin, J. D.; Newton, A. C.; Tsien, R. Y. *Science* **2002**, *296*, 913.
(5) Levental, I.; Lingwood, D.; Grzybek, M.; Coskun, Ü.; Simons, K. *Proc. Natl. Acad. Sci. U.S.A.* **2010**, *107*, 22050.
(6) Mccabe, J. B.; Berthiaume, L. G. *Mol. Biol. Cell* **2001**, *12*, 3601.
(7) Zhang, W.; Trible, R. P.; Samelson, L. E. *Immunity* **1998**, *9*, 239.
(8) Simons, K.; Ikonen, E. *Nature* **1997**, *387*, 569.
(9) Prior, I. A.; Muncke, C.; Parton, R. G.; Hancock, J. F. *J. Cell Biol.* **2003**, *160*, 165.
(10) Henis, Y. I.; Hancock, J. F.; Prior, I. A. *Mol. Membr. Biol.* **2008**, *26*, 80.
(11) Omerovic, J.; Prior, I. A. *FEBS J.* **2009**, *276*, 1817.
(12) Hancock, J. F. *Nat. Rev. Mol. Cell Biol.* **2003**, *4*, 373.
(13) Subramanian, K.; Dietrich, L. E. P.; Hou, H.; LaGrassa, T. J.; Meiringer, C. T. A.; Ungermann, C. *J. Cell Sci.* **2006**, *119*, 2477.
(14) Liang, X.; Nazarian, A.; Erdjument-Bromage, H.; Bornmann, W.; Tempst, P.; Resh, M. D. *J. Biol. Chem.* **2001**, *276*, 30987.
(15) Hancock, J. F. *Nat. Rev. Mol. Cell Biol.* **2006**, *7*, 456.
(16) Pike, L. J. *J. Lipid Res.* **2006**, *47*, 1597.
(17) Munro, S. *Cell* **2003**, *115*, 377.
(18) Magee, T.; Seabra, M. C. *Curr. Opin. Cell Biol.* **2005**, *17*, 190.
(19) Groves, J. T.; Kuriyan, J. *Nat. Struct. Mol. Biol.* **2010**, *17*, 659.
(20) Hartman, N. C.; Groves, J. T. *Curr. Opin. Cell Biol.* **2011**, 370.
(21) Varma, R.; Mayor, S. *Nature* **1998**, *394*, 798.
(22) Sengupta, P.; Jovanovic-Talisman, T.; Skoko, D.; Renz, M.; Veatch, S. L.; Lippincott-Schwartz, J. *Nat. Methods* **2011**, *8*, 969.
(23) Bethani, I.; Skånland, S. S.; Dikic, I.; Acker-Palmer, A. *EMBO J.* **2010**, *29*, 2677.
(24) Grecco, H. E.; Schmick, M.; Bastiaens, P. I. H. *Cell* **2011**, *144*, 897.
(25) Hashimoto-Tane, A.; Yokosuka, T.; Ishihara, C.; Sakuma, M.; Kobayashi, W.; Saito, T. *Mol. Cell. Biol.* **2010**, *30*, 3421.
(26) Saito, T.; Yokosuka, T.; Hashimoto-Tane, A. *FEBS Lett.* **2010**, *584*, 4865.
(27) Bromley, S. K.; Burack, W. R.; G, K.; Somersalo, K.; Sims, T. N.; Sumen, C.; Davis, M. M.; Shaw, A. S.; Allen, P. M.; Dustin, M. L. *Annu. Rev. Immunol.* **2001**, *19*, 375.
(28) Melkonian, K. A.; Ostermeyer, A. G.; Chen, J. Z.; Roth, M. G.; Brown, D. A. *J. Biol. Chem.* **1999**, *274*, 3910.
(29) Arni, S.; Keilbaugh, S. A.; Ostermeyer, A. G.; Brown, D. A. *J. Biol. Chem.* **1998**, *273*, 28478.
(30) Heerklotz, H. *Biophys. J.* **2002**, *83*, 2693.
(31) Lichtenberg, D.; Goñi, F. M.; Heerklotz, H. *Trends Biochem. Sci.* **2005**, *30*, 430.
(32) Veatch, S. L.; Keller, S. L. *Phys. Rev. Lett.* **2002**, *89*, 268101.
(33) Veatch, S. L.; Keller, S. L. *Biophys. J.* **2003**, *85*, 3074.
(34) Baumgart, T.; Hess, S. T.; Webb, W. W. *Nature* **2003**, *425*, 821.
(35) Veatch, S. L.; Cicuta, P.; Sengupta, P.; Honerkamp-Smith, A.; Holowka, D.; Baird, B. *ACS Chem. Biol.* **2008**, *3*, 287.
(36) Baumgart, T.; Hammond, A. T.; Sengupta, P.; Hess, S. T.; Holowka, D. A.; Baird, B. A.; Webb, W. W. *Proc. Natl. Acad. Sci. U.S.A.* **2007**, *104*, 3165.
(37) Hammond, A. T.; Heberle, F. A.; Baumgart, T.; Holowka, D. A.; Baird, B. A.; Feigenson, G. W. *Proc. Natl. Acad. Sci. U.S.A.* **2005**, *102*, 6320.
(38) Veatch, S. L.; Keller, S. L. *Biochim. Biophys. Acta* **2005**, *1746*, 172.
(39) London, E. *Curr. Opin. Struct. Biol.* **2002**, *12*, 480.
(40) Johnson, S. A.; Stinson, B. M.; Go, M. S.; Carmona, L. M.; Reminick, J. I.; Fang, X.; Baumgart, T. *Biochim. Biophys. Acta* **2010**, *1798*, 1427.
(41) Glebov, O. O.; Nichols, B. J. *Nat. Cell Biol.* **2004**, *6*, 238.
(42) Edidin, M. *Annu. Rev. Biophys. Biomol. Struct.* **2003**, *32*, 257.
(43) Mayor, S.; Rao, M. *Traffic (Copenhagen, Denmark)* **2004**, *5*, 231.
(44) Douglass, A. D.; Vale, R. D. *Cell* **2005**, *121*, 937.
(45) Kenworthy, A. K.; Nichols, B. J.; Remmert, C. L.; Hendrix, G. M.; Kumar, M.; Zimmerberg, J.; Lippincott-Schwartz, J. *J. Cell Biol.* **2004**, *165*, 735.
(46) Lillemeier, B. F.; Mörtelmaier, M. A.; Forstner, M. B.; Huppa, J. B.; Groves, J. T.; Davis, M. M. *Nat. Immunol.* **2010**, *11*, 90.
(47) Müller, B. K.; Zaychikov, E.; Bräuchle, C.; Lamb, D. C. *Biophys. J.* **2005**, *89*, 3508.
(48) Schwille, P.; Meyer-Almes, F. J.; Rigler, R. *Biophys. J.* **1997**, *72*, 1878.
(49) Lamb, D. C.; Müller, B. K.; Bräuchle, C. *Curr. Pharma. Biotechnol.* **2005**, *6*, 405.
(50) Lin, W.-C.; Yu, C.-H.; Triffo, S.; Groves, J. T. *Curr. Protoc. Chem. Biol.* **2010**, *2*, 235.
(51) Nye, J. A.; Groves, J. T. *Langmuir* **2008**, *24*, 4145.
(52) Legler, D. F.; Doucey, M.-A.; Schneider, P.; Chapatte, L.; Bender, F. C.; Bron, C. *FASEB J.* **2005**, *19*, 73.
(53) Ries, J.; Schwille, P. *Phys. Chem. Chem. Phys.* **2008**, *10*, 3487.
(54) Bacia, K.; Schwille, P. *Nat. Protoc.* **2007**, *2*, 2842.
(55) Wohland, T.; Rigler, R.; Vogel, H. *Biophys. J.* **2001**, *80*, 2987.
(56) Lakowicz, J. R. *Principles of Fluorescence Spectroscopy*, 3rd ed.; Springer: New York, 2006; p 105.
(57) Shaner, N. C.; Campbell, R. E.; Steinbach, P.; Giepmans, B. N. G.; Palmer, A. E.; Tsien, R. Y. *Nat. Biotechnol.* **2004**, *22*, 1567.
(58) Jang, J. H.; Hanash, S. *Proteomics* **2003**, *3*, 1947.
(59) von Haller, P. D.; Donohoe, S.; Goodlett, D. R.; Aebersold, R.; Watts, J. D. *Proteomics* **2001**, *1*, 1010.
(60) Brown, D. A.; Rose, J. K. *Cell* **1992**, *66*, 533.
(61) Brown, D. A.; London, E. *Annu. Rev. Cell Dev. Biol.* **1998**, *14*, 111.
(62) Owen, D. M.; Rentero, C.; Rossy, J.; Magenau, A.; Williamson, D.; Rodriguez, M.; Gaus, K. *J. Biophoton.* **2010**, *3*, 446.
(63) Eggeling, C.; Ringemann, C.; Medda, R.; Schwarzmann, G.; Sandhoff, K.; Polyakova, S.; Belov, V. N.; Hein, B.; Middendorff, C.; von; Schönle, A.; Hell, S. W. *Nature* **2009**, *457*, 1159.
(64) Kaiser, H.-J.; Lingwood, D.; Levental, I.; Sampaio, J. L.; Kalvodova, L.; Rajendran, L.; Simons, K. *Proc. Natl. Acad. Sci. U.S.A.* **2009**, *106*, 16645.

NOTE ADDED AFTER ASAP PUBLICATION

This paper was published ASAP on June 14, 2012. The title has been restored to its originally accepted form. The revised version was posted on June 20, 2012.

dx.doi.org/10.1021/ja300374c | J. Am. Chem. Soc. 2012, 134, 10833−10842